

Instructional Video Generation

Yayuan Li¹ Zhi Cao¹ Jason J. Corso^{1,2}
¹University of Michigan ²Voxel51

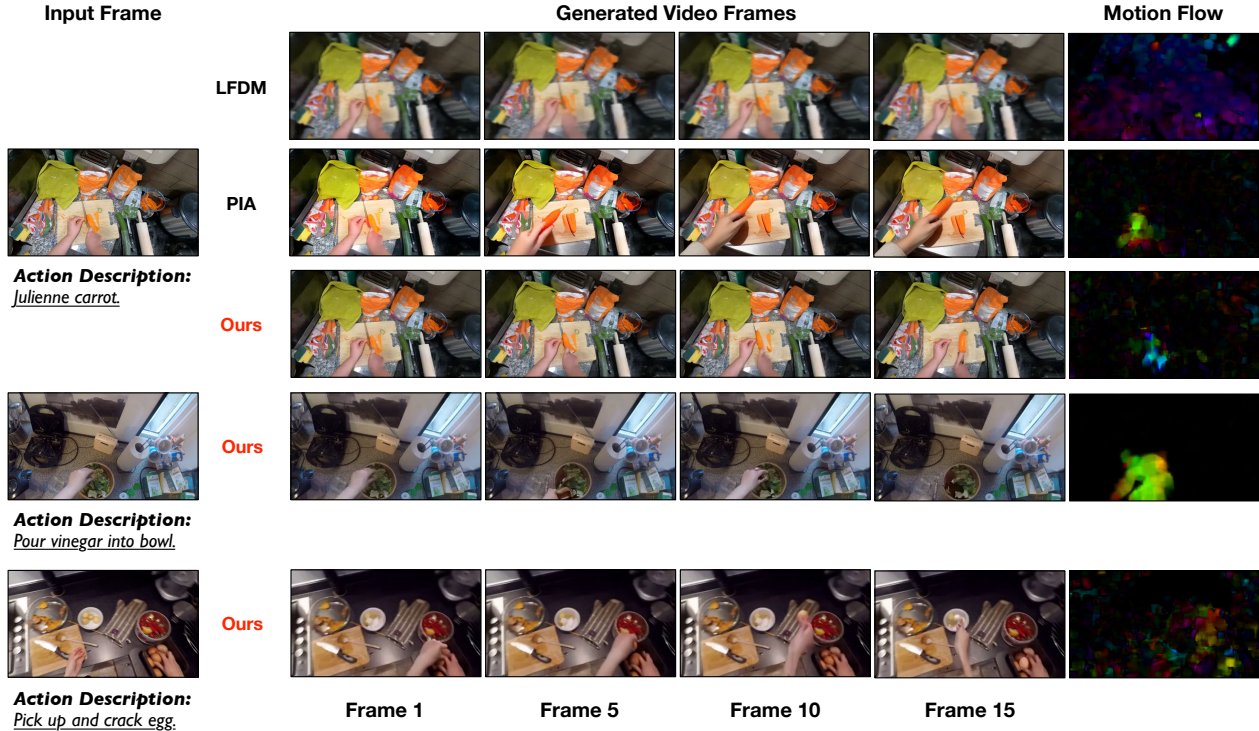


Figure 1. Illustration of our proposed problem—Instructional Video Generation (IVG). The inputs are an image providing visual context and an action text prompt describing the task to be demonstrated. The outputs are generated video frames showing the action through detailed hand motion. Challenges include cluttered backgrounds and subtle, task-specific hand movements. Compared to baselines, which introduce unnecessary background changes, our method focuses on the specific region where the action occurs. We visualize these differences by computing the optical flow of the generated frames, showing clear improvements in action localization. Our approach also produces more accurate hand motions, while baselines fail due to distractions from cluttered backgrounds and a lack of hand structure guidance. This figure highlights how our method capture the subtle motion localized to the appropriate region.

Abstract

Despite the recent strides in video generation, state-of-the-art methods still struggle with elements of visual detail. One particularly challenging case is the class of egocentric instructional videos in which the intricate motion of the hand coupled with a mostly stable and non-distracting environment is necessary to convey the appropriate visual action instruction. To address these challenges, we introduce a new method for instructional video generation. Our diffusion-based method incorporates two distinct innovations. First,

we propose an automatic method to generate the expected region of motion, guided by both the visual context and the action text. Second, we introduce a critical hand structure loss to guide the diffusion model to focus on smooth and consistent hand poses. We evaluate our method on augmented instructional datasets based on EpicKitchens and Ego4D, demonstrating significant improvements over state-of-the-art methods in terms of instructional clarity, especially of the hand motion in the target region, across diverse environments and actions.¹

¹Video results can be found on the [project webpage](#)

1. Introduction

Instructional videos—videos demonstrating sequences of goal-oriented actions involving dexterous hand motion and interaction with the environment [18, 24, 79, 96]—are the de facto contemporary source for humans when learning new skills or refreshing forgotten ones, such as cooking a certain dish or fixing a broken bicycle [2, 3, 6, 35, 72, 73, 78, 85]. They have demonstrated extensive effectiveness in robot learning [4, 11, 15, 23, 34, 37, 49, 58, 87, 87, 88, 94].

However, instructional videos are rarely available in arbitrary working environments where humans or robots operate. While humans can readily adapt to environmental variations, such changes pose significant challenges for robots or other AI agents, limiting the applicability to broader scenarios [71]. Recent work has explored the generation of instructional images [39, 71] or the retrieval of existing videos for reference [3, 25], with limited success. But, images do not highlight the temporal flow of actions, requiring challenging extrapolation, and the retrieved videos have various distractions, such as a different visual appearance of target objects, different view points, and background variations, which increases cognitive load for human learners [10] and is harmful to robot policy learning [11, 34, 49].

To address this gap, we directly generate instructional videos. Concretely, maintaining the same protocol as the previous instructional image generation work [39, 71], we describe the target instructional action in natural language text and provide one RGB image depicting the visual environment. As shown in Fig. 1, the generated instructional videos are expected to showcase the consistent motion of the target action with a clear motion subject (the hand) appearance. At the same time, the generated videos should not introduce any unnecessary distractions: e.g., after “cutting a carrot,” the carrot should actually be rendered as a bunch of carrot pieces, but the rest of the environment should not be changed (no object hallucinations in the background, no lighting changes, no camera movements, and so on).

On the technical side, the solution to this problem aligns with the trajectory of image-and-text to video (IT2V) works [7, 16, 17, 20, 22, 26, 30, 32, 43, 55, 57, 65, 66, 80, 82, 91, 93] since they have the same input (single image and text) and output (video) modalities as our problem setting. However, there are critical differences between IT2V and instructional video generation (IVG) that, despite the advances in IT2V, make IVG a challenge. These include the ability to avoid distracting content and to generate high-quality hand motions and realistic appearances, which we describe in more detail next.

First, existing IT2V generation works focus on videos that have scenery-, character- or object-centric content. In

those videos, the Region of Motion (RoM)—the area in the input image where the pixel content should be “edited” for the target actions—dominates because of the large target size and the typically clean background (for character- and object-centric cases). In contrast, instructional videos usually have fine-grained motion with a small subject (e.g., hand) carrying out a well-defined task, surrounded by often very cluttered backgrounds. Unfortunately, as shown in Fig. 1 contemporary IT2V methods lead to distracting content like a hallucination in the background (e.g., a hand pops up in the background and new objects in the background).

Even though some work has identified these challenges in hard samples, they rely on the extra user input of the RoM mask to prevent the distracting content out of RoM [17] or even motion flow [32, 43, 91], which do not scale. On the other hand, recent works about robotic policy learning via video generation [19, 70, 88] mitigate the hallucination issue by fitting a huge amount of training samples, but they still struggle with camera movement in the generated videos because the training videos contain significant amounts of camera movement, which is known to be highly distracting for learners [8, 36].

Second, generating high-quality articulated hand motion in instructional videos is important but hard. To be useful for later learning, the generated hand must be consistent—smooth and non-flickering hand pose in consecutive frames. And, yet, consistent is not enough: it must also capture the semantics of the instructional task described by the prompt, showcasing the correct motion and interaction with environment and the objects within it, as depicted in the input image. Existing visual generation techniques are known to struggle with these critical IVG needs [47, 53, 56, 89].

To overcome these technical challenges, we propose a novel IVG method that automatically infers the RoM and incorporates a hand structure loss with a 3D diffusion model (space-time) as the backbone [31, 62]. We design a two-stage approach for IVG. In the first stage, we learn a model to infer the RoM so that the 3D diffusion can leverage this spatial information; this model must incorporate information from both the prompt and the input image to ensure the appropriate regional focus is made. In the second stage, we augment the 3D diffusion backbone with an innovative hand structure loss, since the consistency of motion and appearance of the hand is critical in IVG. The hand structure loss is computed from the similarity between the ground truth and generated hand key points, which encourages the generated videos to have realistic and consistent hand motion. We explain the details about our method in Sec. 3.

We augment two previous instructional image generation datasets [39] based on Ego4D [24] and EpicKitchens [18] for evaluation. In addition to various standard video generation metrics, we propose two additional metrics focusing

on good RoM and hand appearance. We first compare with SOTA video generation methods to show the effectiveness of our proposed method, demonstrating our method’s strong performance for IVG [17, 88, 90].

Then, we take a closer look at model performance along key axes: we investigate the performance of hard samples—samples with large RoM and motion complexity defined by hand movement. We show that our model outperforms SOTA baselines on these hard samples. 2) We compare different approaches of identifying the RoM and demonstrate that our proposed gives the best results.

In summary, we address the problem of generating instructional videos from a single RGB image and text prompt. Our contributions are two-fold:

- We identify the unique aspects of instructional video generation (IVG) and propose a new method that is able to address the unique challenges of IVG.
- We demonstrate that our new IVG method is able to outperform state of the art video generation from image and text-prompt methods, along all measurement axes.

We will release code and benchmark.

2. Related Work

Instructional Videos are distinct from general-purpose videos as they focus on task-specific actions with clear procedural steps and precise hand-object interactions [51]. Prominent datasets like HowTo100M [51], Recipe1M [50], and YouCook2 [97] emphasize instructional content, particularly in culinary tasks where detailed hand movements are crucial. Other datasets, such as EPIC-Kitchens [18] and Ego4D [24], focus on egocentric views, providing annotations that capture the nuances of task-specific actions.

The challenges in instructional videos, such as cluttered backgrounds and fine-grained hand-object interactions, have led to specialized research on procedural video understanding. Key efforts like Assembly101 [64], Meccano [60], and HoloAssist [77] explore diverse instructional settings, advancing multimodal understanding. These datasets showcase the need for generation methods that prioritize action precision and task relevance while addressing the unique modeling challenges of instructional videos.

Video Generation, particularly image-and-text to video (IT2V) methods, has advanced significantly through generative models like diffusion models [62]. IT2V methods, including TI2V-Zero [55] and PIA [93], extend text-to-image (T2I) models [62, 63] to produce videos conditioned on images and text. Works like VideoCrafter [13, 14] and Drag-NUWA [91] focus on general-purpose synthesis but are less effective for instructional video generation (IVG), which requires precise hand-object interactions and background consistency.

Broader efforts, such as UniSim [88] explore action-conditioned synthesis across tasks but rely on large-scale

egocentric datasets, retaining distracting camera movements [8, 36]. On the other hand, innovations like Make-A-Video [67] enhance T2V capabilities but fall short in addressing IVG’s specific needs. In contrast, our method bridges these gaps by focusing on high-quality, subtle hand motions and avoiding distracting artifacts, setting a new standard for instructional video generation.

3. Instructional Video Generation

Problem Statement Formally, we define the instruction video generation (IVG) problem as follows. Given an egocentric RGB image $I \in \mathbb{R}^{H \times W \times 3}$ in which we assume there is a user ready to perform an action, and given a text prompt to describe the action T , a method Ψ is expected to output a RGB video clip $V \in \mathbb{R}^{L \times H \times W \times 3}$ demonstrating how the action T is done in the same visual environment shown in I . We reserve notation I for this purpose and refer to it as I or *visual context* in the paper.

Method Overview To tackle this image-text to video generation problem specifically with instructional content, we introduce two main innovations, leveraging existing video generation workflow as a base. First, we propose a backbone-shared two-stage approach. Stage one learns to automatically determine the Region of Motion—the spatial region in the input image where the target motion occurs; Then, stage two, which uses the same backbone, is conditioned on this region of motion input for instructional video generation. This spatially cued approach is specifically pertinent to IVG as it avoids the generation of distractions out of the action’s scope. Second, we propose a novel hand structure loss tailored to IVG. This loss greatly helps the generated video deliver higher quality of instructional information since hand is the key element when demonstrating actions in this scenario.

3.1. Region of Motion Aware Two-Stage IVG

We introduce our two-stage approach that improves video generation by first learning to determining Region of Motion (RoM). Given a backbone diffusion pipeline, we first train it to generate an RoM mask $M \in \mathbb{R}^{H \times W}$. Then, at stage 2, we continue to train the model to directly generate the instructional video when conditioned on the mask M generated by the stage 1 model.

3.1.1. Stage 1: Learn to generate region of motion mask

RoM Mask Pseudo Annotation Existing relevant datasets lack manual annotation for the RoM mask because it is expensive. We hence automatically annotate the region of motion using state of the art hand detection [48], as shown in Fig. 2 (b). Concretely, given a training video $V \in \mathbb{R}^{(L+1) \times H \times W \times 3}$ (including context image as the first frame), we apply a well-trained hand keypoint detector \mathbf{H} that outputs, for each frame $l = [0, 1, 2, \dots, L]$, a set of

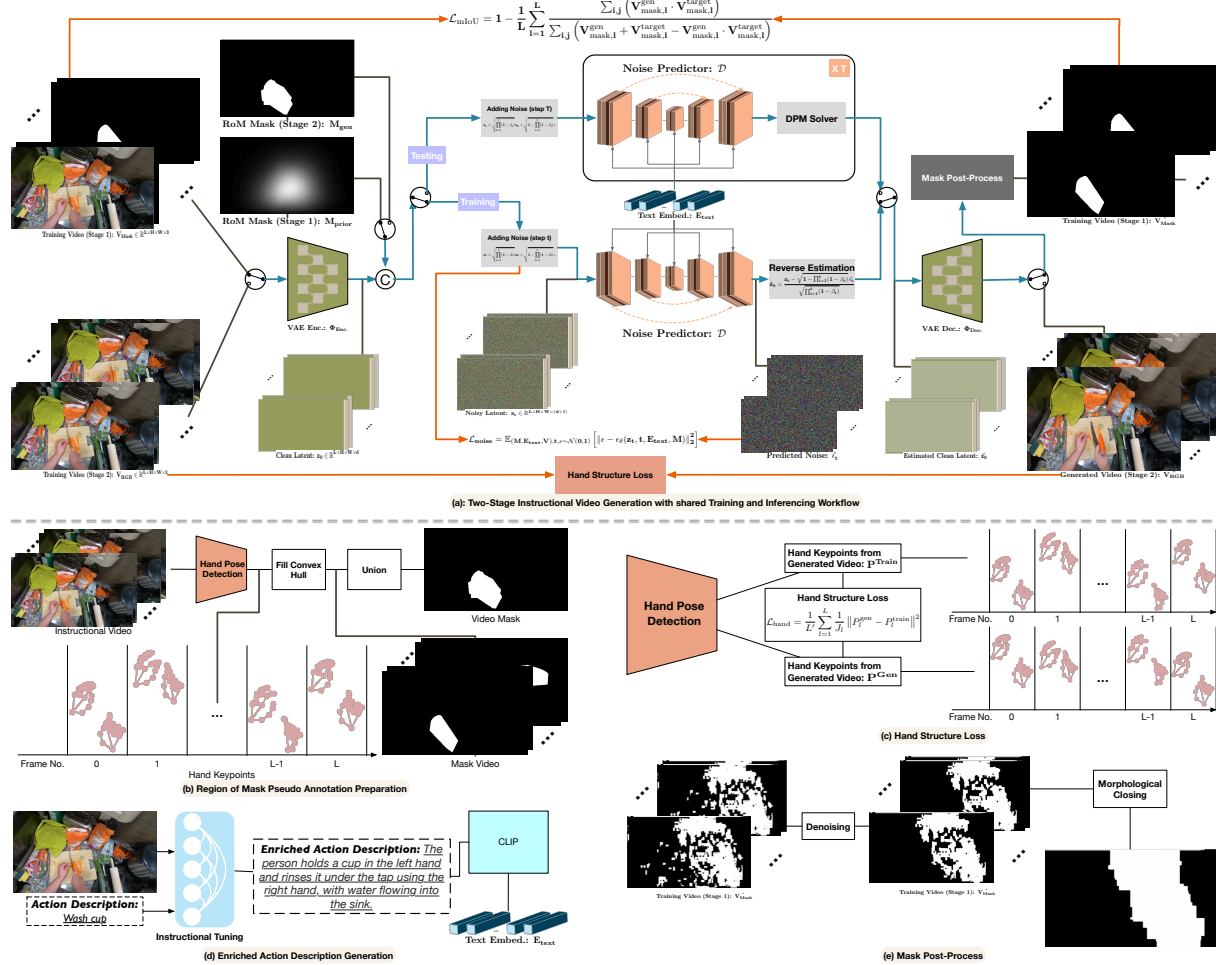


Figure 2. Method Overview: Our two-stage framework first predicts a Region of Motion (RoM) mask to localize task-relevant areas, then guides video generation to capture accurate and subtle hand movements, enhancing the clarity and focus of instructional content.

hand keypoints $P_l \in \mathbb{R}^{J_l \times 2}$ where J_l is the number of 2D key points detected for frame l . For each P_l , we do Convex Hull Filling to delimit a region as the action region mask M_l at frame l . Then we apply union over masks for all frames to produce the final Region of Motion mask $M_{video} \in [0, 1]^{H \times W}$.

Training With the pseudo ground truth RoM mask for each frame, we can train a video generation model that can generate RoM mask from the context image and action text. We adapt SOTA video latent diffusion works [21, 54, 80]. The essence of these model is a denoising function f_M (rendered as a 3D UNet, in our case), and conditioned on the action text, which we describe first.

Let E_{text} represent the *action text embedding* from the input action text description T . As shown in Fig. 2 (d), we leverage a pre-trained instructional tuning module [39], to generate descriptive actions from the input original action text because of the strong evidence that conditioned denois-

ing models (diffusion) perform better when there is rich description of the motion [9, 39, 71, 92]. Then, we use the CLIP text embedding [59] to generate the final action text embedding $E_{text} \in \mathbb{R}^{N \times d}$ where N is the number of tokens and d is the feature dimension.

Given the action text embedding E_{text} , let us now consider the diffusion process, as shown in Fig. 2. Concretely, given a RGB instructional video $V_{RGB} \in \mathbb{R}^{(L+1) \times H \times W \times 3}$ (including the context image), we first prepare the mask video for training: $V_{Mask} \in \mathbb{R}^{(L+1) \times H \times W \times 3}$. To supply the visual context to the diffusion model, we make the first frame V_{Mask}^0 to be the same as V_{RGB}^0 — the I in problem definition. We use the pseudo ground truth mask for the rest of the frames in V_{RGB}^l as V_{Mask}^l ($l = 1, 2, 3, \dots, L$). Since we used a shared workflow for both stages, we triple the each mask to align with the number of channels in RGB frames.

Then, in stage 1, the training video V_{Mask} is processed

by a pretrained VAE encoder [61, 62] frame by frame, aligning with previous works [17, 21, 31, 68, 80]. This stage converts information to latent space and produces a clean latent video $z_0 \in \mathbb{R}^{(L+1) \times H \times W \times c}$, where c is the latent space dimension. For each training forward step, following standard practices [45, 46, 62], we prepare the noisy latent video z_t for $t \in 1, \dots, \tau$ where τ is a predefined max step, according to standard noise-adding process [29, 56]:

$$z_t = \sqrt{\prod_{i=1}^t (1 - \beta_i)} z_0 + \sqrt{1 - \prod_{i=1}^t (1 - \beta_i)} \epsilon, \quad (1)$$

where β_i is a predefined coefficient that controls noise intensity at step i and $\epsilon \sim \mathcal{N}(0, \mathbf{I})$ is the sampled noise.

Then, we use a 3D UNet-based Noise Predictor \mathbf{D} commonly used in existing work [21, 31, 62, 68, 80] to predict the added noise as a core module of the denoising process. This off-the-shelf 3D UNet structure takes the current noisy latent sample z_t and conditions on the Action Text Embedding E_{text} for generation. Each of its blocks contains convolution layers [41] for spatial information extraction at per frame level, temporal convolution layers [40, 75] and temporal attention layers [86] for information fusion across all timestamps at video level, and extra cross attention layers [76] to fuse information from text embedding E_{text} .

With the predicted noise $\hat{\epsilon}_t$ generated by \mathbf{D}_1 , the estimated latent clean video \hat{z}_0 can be computed from z_t the inverse version of Eq. (1), as explained in [29, 56]. Naturally, the estimated video in pixel space \hat{V} is decoded from \hat{z}_0 by the pretrained VAE decoder frame by frame.

Note that we optimize \mathbf{D}_1 specifically for IVG, by, for example enforcing a hand structure loss during training (discussed later in Sec. 3.2) along with standard noise prediction loss.

Inference Recall, inference is given the visual context image I and action text description T as input; its goal is to output a video with L frames that showcase the action from T in the given visual context I . Fig. 2 visualizes this.

Starting with visual context I , we produce $z_{context}$ from a VAE encoder pre-trained by Stable Diffusion v1.5 [62]. Then, following [17], we duplicate $z_{context}$ for L times and apply Eq. (1) at the max noise step τ to produce the initial noisy latent video z'_T as the beginning of denoising process. Unlike the training process the denoising process during inference iterates τ steps for better performance. At each denoising step t the trained model \mathbf{D}_1 conditionally predicts the noise $\hat{\epsilon}_t$ from z'_T , the same as training process.

We diverge from training practice when we apply the DPM solver [45, 46] to calculate the noise latent video at previous timestamp z'_{t-1} iteratively for τ times instead of at step 0 directly. This choice reflects our preference for generation quality over denoising speed during inference, as the DPM solver is effective despite its higher time cost. Af-

ter τ steps of denoising, an estimated clean latent video z'_0 is produced. The pretrained VAE decoder [62] is again applied per-frame to produce the predicted action region mask at each frame in pixel space.

As shown in Fig. 2 (e), a post-process is proposed to make cleaner action region masks $M_l \in \mathbb{R}^{H \times W \times 3}$. We remove small isolated regions with connected component analysis and morphology. In the end, we apply spatial union over all M_l to produce the predicted Region of Motion mask M_{Video} for the input context image and action.

3.1.2. Stage 2: Instructional Video Generation

Stage 1 produces a noise prediction model \mathbf{D}_1 that is trained to be able to predict a Region of Motion mask M_{Video} given the input context image I and action description T . Stage 2 leverages the outcomes of stage 1 to generate the instructional video that clearly demonstrate the action while preserving the visual context.

Therefore, following the same workflow as introduced in the stage 1, we conduct following changes to generate the RGB instructional video as shown in the Fig. 2 (a). First, we use the training video $V_{RGB} \in \mathbb{R}^{(L+1) \times H \times W \times 3}$ (including the context image) to train the noise predictor \mathbf{D}_2 conditioned on the mask \hat{M}_{gen} predicted with \mathbf{D}_1 . In the end, we use different sets of objectives to optimize stage 2 as described below in Sec. 3.3.

During inference, given the visual context image I and the action description T , we first infer the RoM mask M_{gen} , using noise predictor \mathbf{D}_1 trained from stage one. Then we finish the IVG to infer the output video \hat{V}_{RGB} using \mathbf{D}_2 . Our extensive experiments show the high impact of the RoM in instructional video generation Sec. 4.

3.2. Hand Structure Loss

High-quality hand motion is vital for instructional videos, as it conveys essential information for demonstrating action execution [33]. We address this need with a new hand structure loss function, which we denote \mathbf{L}_{hand} . Our approach is lightweight and organically fuses in the main training process without requiring extra heavy post-processing model preparation. We are not aware of other video generation work that explicitly focuses on optimizing hand generation within the same generation model; those we are aware of require a separate model and heavy post processing to optimize hand quality [47, 53, 89].

As shown in Fig. 2 (c), we compute the hand structure loss between the generated instructional video $V_{RGB}^{gen} \in \mathbb{R}^{(L+1) \times H \times W \times 3}$ from stage 2 and the input training video $V_{RGB}^{train} \in \mathbb{R}^{(L+1) \times H \times W \times 3}$. Concretely, we apply a state of the art hand pose detector \mathbf{H} on both videos [48]. \mathbf{H} produces the coordinates of hand joints $P_l \in \mathbb{R}^{J_l \times 2}$ for each frame l while considering the temporal information in the video. J_l denotes the number of detected keypoints in frame l . This process yields detected hand pose sequences in the

Dataset	Method	HS-Err. \downarrow	GT-Frame		GT-Video		Consistency	Semantic	
			FID \downarrow	CLIP \uparrow	FVD \downarrow	EgoVLP \uparrow		CLIP \uparrow	CLIP \uparrow
EpicKitchens	LFDM [54]	0.01987	39.37	92.414	129.80	0.354	0.9826	28.37	0.235
	AA [17]	0.01908	5.49	95.882	171.29	0.338	0.9843	29.97	0.295
	AVDC [90]	0.01969	140.34	89.176	81.39	0.197	0.9582	24.66	0.116
	PIA [93]	0.01826	24.70	94.455	212.88	0.361	0.9849	30.06	0.294
	Ours	0.01512	5.27	95.904	101.89	0.377	0.9896	31.14	0.298
Ego4D	LFDM [54]	0.02127	50.67	92.037	126.71	0.535	0.9821	26.93	0.221
	AA [17]	0.02393	21.83	96.472	129.60	0.642	0.9894	28.56	0.260
	AVDC [90]	0.02117	144.91	88.160	107.82	0.261	0.9722	24.17	0.155
	PIA [93]	0.02393	34.62	94.574	104.38	0.603	0.9746	29.15	0.219
	Ours	0.01939	21.51	96.506	103.15	0.664	0.9873	28.63	0.263
Motion Intensive	LFDM [54]	0.02053	56.95	92.540	137.44	0.303	0.9825	28.39	0.210
	AA [17]	0.01764	23.93	95.909	115.14	0.368	0.9845	30.07	0.276
	AVDC [90]	0.02143	148.11	89.327	85.97	0.204	0.9579	24.60	0.102
	PIA [93]	0.01940	40.97	94.482	217.59	0.330	0.9719	30.09	0.280
	Ours	0.01663	23.79	95.885	114.52	0.371	0.9849	31.12	0.327

Table 1. Quantitative results on EpicKitchens [18], Ego4D [24] and a Motion Intensive subset of EpicKitchens. Our method outperforms all baselines across all metrics on at least one dataset.

generated video $P^{gen} = P_1, P_2, \dots, P_L$ and in the training video $P^{train} = P_1, P_2, \dots, P_L$. We use the MSE between these two poses sequences as the loss value:

$$\mathcal{L}_{\text{hand}} = \frac{1}{L'} \sum_{l=1}^L \frac{1}{J_l} \|P_l^{gen} - P_l^{train}\|^2 \quad , \quad (2)$$

where L' is the number of frames the loss is computed on, $P_{l,j}^{\{gen,train\}}$ represents the coordinates of the j -th hand keypoint in frame l . For frame l , when detected keypoints J_l is not the same for V_{RGB}^{gen} and V_{RGB}^{train} (i.e., there is no detectable hand in the generated video), we set the coordinates of the missing joints in P^{gen} as 0 so that the noise predictor \mathbf{D}_2 will be optimized for such samples as well.

Notably, the hand detector \mathbf{H} is frozen. Incorporating this loss hence encourages the noise predictor \mathbf{D}_2 to focus on the hand structure when modeling the distribution of pixels in the training videos.

3.3. Final Loss Portfolio

The final loss function contains a standard noise prediction loss $\mathcal{L}_{\text{noise}}$ and a Mean Intersection of Union (mIoU) loss $\mathcal{L}_{\text{mIoU}}$ or a hand structure loss $\mathcal{L}_{\text{hand}}$, for stage 1 or 2, respectively. $\mathcal{L}_{\text{noise}}$ optimizes the noise predictor \mathbf{D} via the generated noise in the latent space. The hand structure loss $\mathcal{L}_{\text{hand}}$ or the mIoU loss $\mathcal{L}_{\text{mIoU}}$ optimize the noise predictor via the reconstructed videos.

For stage one, we apply a mIoU loss $\mathcal{L}_{\text{mIoU}}$ in addition to $\mathcal{L}_{\text{noise}}$ to have the final loss:

$$\mathcal{L}_{\text{stage1}} = \mathcal{L}_{\text{noise}} + \beta \mathcal{L}_{\text{mIoU}} \quad (3)$$

where β is a hyperparameter tuned empirically. The Mean Intersection over Union (mIoU) loss is defined as

$$\mathcal{L}_{\text{mIoU}} = 1 - \frac{1}{L+1} \sum_{l=1}^L \frac{\sum_{i,j} (V_{\text{mask},l}^{\text{gen}} \cdot V_{\text{mask},l}^{\text{target}})}{\sum_{i,j} (V_{\text{mask},l}^{\text{gen}} + V_{\text{mask},l}^{\text{target}} - V_{\text{mask},l}^{\text{gen}} \cdot V_{\text{mask},l}^{\text{target}})}, \quad (4)$$

where $V_{\text{mask},l}^{\text{gen}}$ and $V_{\text{mask},l}^{\text{target}}$ are the generated and target binary masks for frame l , summed over spatial dimensions i and j . L denotes the number of frames in the training video except the context image.

We adapt existing standard noise prediction loss to minimize the estimation of the similarity between the standard Gaussian noise and our conditionally predicted noise from our trained noise predictor \mathbf{D} . Formally, it is defined as:

$$\mathcal{L}_{\text{noise}} = \mathbb{E}_{(M, E_{\text{text}}, V), t, \epsilon \sim \mathcal{N}(0, 1)} [\|\epsilon - \epsilon_{\theta}(z_t, t, E_{\text{text}}, M)\|^2] \quad (5)$$

where M is the RoM mask, V is the training video, t is the sampled noise-adding timestamp, ϵ is the sampled noise and ϵ_{θ} is the noise conditionally predicted by the noise predictor with parameters θ at the training step.

Likewise, we have the final loss for stage 2 training:

$$\mathcal{L}_{\text{stage2}} = \mathcal{L}_{\text{noise}} + \alpha \mathcal{L}_{\text{hand}} \quad , \quad (6)$$

with the hyperparameter α .

4. Experiments

4.1. Metric

First, we evaluate the similarity between the generated videos and ground truth videos. Following previous video generation works, we perform image-to-image FID [28]

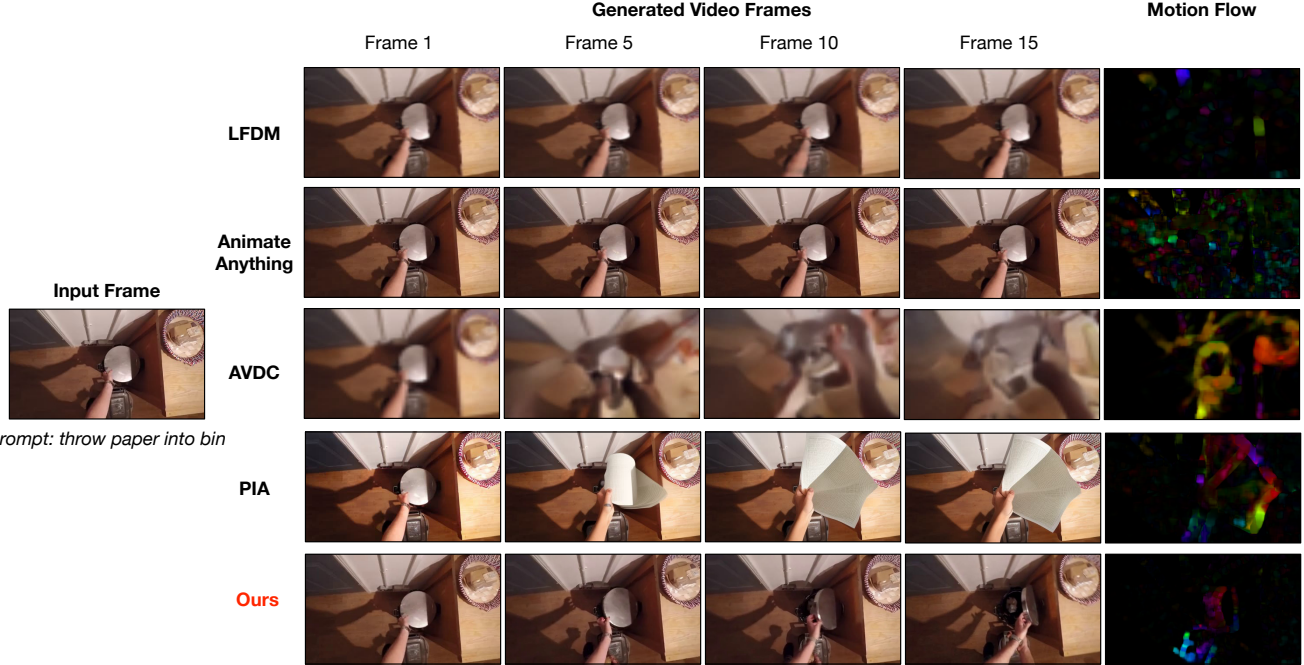


Figure 3. Qualitative results comparing with baselines. Our method generates instructional videos that contain subtle hand motion that corresponds to the action description. This is because our method focus on the effective motion region instead of cluttered background and our method is optimized with a tailored hand structure loss. The optical flow of the generated video provides more straightforward visualization and yield the same conclusion. Please see more video results in supplementary materials.

No.	Mask	Hand	HS-Err. \downarrow	GT-Frame		GT-Video		Consistency		Semantic	
				FID \downarrow	CLIP \uparrow	FVD \downarrow	EgoVLP \uparrow	CLIP \uparrow	CLIP \uparrow	CLIP \uparrow	BLIP \uparrow
1	White mask	\times	0.01908	5.497	95.882	171.29	0.338	0.9843	29.970	0.295	
2	GT mask	\times	0.01935	5.287	95.894	102.43	0.380	0.9842	30.05	0.297	
3	Prior Mask	\checkmark	0.01670	5.285	95.883	137.01	0.354	0.9869	30.045	0.297	
4	Stage 1	\times	0.01940	5.570	95.898	124.42	0.197	0.9881	29.94	0.296	
5	Stage 1 + Hand	\checkmark	0.01512	5.272	95.904	101.89	0.377	0.9896	30.055	0.298	

Table 2. Ablation study on the EpicKitchens dataset [18], examining the impact of Region of Motion (RoM) mask generation (“Mask”) and Hand Structure Loss (“Hand”) on model performance. Each component is evaluated individually and in combination, demonstrating their contributions to improved visual quality and consistency across frames and videos.

and CLIP_{toGT} score (average CLIP similarity between groundtruth and generated frames) [59] as our averaged frame-level similarity. Also to align with previous work [39], we compute FVD [74] and EgoVLP score [39, 44] as video-to-video similarity metrics. For fair comparison, we report evaluation results on latter L frames in the generated and ground truth videos, which do not contain the images corresponds to context image I .

Second, we measure consistency between frames in generated videos via CLIP_{toConsec} score (average CLIP similarity between consecutive frames) [59]. Also, we evaluate the semantic similarity between the prompt text and the generated video. We adopt the CLIP_{toText} score (averaged CLIP similarity between text and generated frames) [81]

and BLIP score [39, 42]. Also, we report Hand Structure Error (HS-Err) which is defined in a similar manner to the hand structure loss Sec. 3.2. For qualitative results, in addition to generated frames, we also present the optical flows over the generated video to compare if the result contains unnecessary motion.

4.2. Baseline

Our baseline methods include LFDM [54], AnimateAnything (AA) [17], AVDC [90], and PIA [93]. LFDM uses a latent flow diffusion model to generate temporally-coherent videos by synthesizing a latent optical flow sequence for the whole frame warping but lacks mechanisms specific to fine-grained hand-object interactions and the correspond-

ing region. AA leverages a motion area mask and strength guidance for open-domain image animation, focusing on general object animation without specialized hand motion guidance. AVDC reformulates video generation as a text-guided policy learning task, creating diverse action-driven videos but without targeted mechanisms for subtle instructional actions. PIA introduces temporal alignment layers and a condition module for personalizing T2I models to animate images with controlled motions, but it does not specifically address the cluttered backgrounds or hand precision required for instructional videos.

As none of these baselines have been applied to instructional video generation (IVG), we fine-tune all baseline models on both the Epic-Kitchen and Ego4D datasets for 50 epochs (200,000 iterations with a batch size of 16) to allow sufficient learning on our benchmark. Further details on training specifics are provided in the supplementary materials.

4.3. Datasets and Implementation Details

Datasets. We perform our experiments on two widely used ego-centric instructional video datasets: Epic-Kitchens-100 [18] and Ego4D [24]. They come with annotations for short video clips of actions (clips lasting a few seconds typically). The key annotations are starting and ending frame of the clip and a short natural language description for the action. Specifically, we use the filtered versions and splits of the two datasets from previous action effect image generation works [39]. They filter out low quality samples like blurry video clips and the clips with stationary actions (e.g., reading book). Based on that, we evenly sample 16 frames from each video where the first frame is the context image I in our problem definition and the remaining 15 frames (i.e., $L = 15$, Sec. 3) comprise the video to be “reconstructed” during training. In the end, the Epic-Kitchens-100 contains 61841 training samples and 8893 test samples and Ego4D contains 85521 training samples and 9931 test samples. We will make all details about this sampling regimen available in code after publication to support comparisons.

Implementation Details. The coefficients in the loss functions are $\alpha = 1$ and $\beta = 0.1$ for Stage 1 and Stage 2, separately. We use mix precision training with bf16. So, although the ground truth masks are initially binary masks, we convert them to floats 0.0 and 1.0. We train our method on $6 \times$ H100 GPUs.

4.4. Comparisons with State of the Art

We report main results in Tab. 1. We outperform all the baselines across all the metrics on at least one dataset. Besides, as shown in Fig. 3, our generated videos contain subtle hand movement that corresponds to the action description. This is because our method is not distracted by

the clutter background as the baseline methods do, which demonstrates to effectiveness of our proposed Region of Motion generation module. The optical flow is shown for a better comparison of the subtle hand motion in the generated videos. These results demonstrate the superior performance of our proposed method of Instructional Video Generation which commonly contains subtle hand motion in a cluttered background. Please check supplementary materials for more results in videos.

Furthermore, we measure the performance on motion-intensive samples. We pick a subset of test samples from test set that have top 10% large pseudo ground truth region of motion mask in EpicKitchens [18]. This can help us understand the performance robustness for motion-intensive samples, as shown in Tab. 1 (Motion-Intensive).

4.5. Ablation Study

As shown in Tab. 2, we validate the effectiveness of the two key components: Region of Motion (RoM) mask generation Sec. 3.1 and Hand Structure Loss Sec. 3.2. Comparing no mask (No. 1) with a groundtruth mask (No. 2) shows that constraining the RoM improves IVG performance. Additionally, generating the RoM mask in Stage One (No. 4) yields comparable results to using the groundtruth mask, demonstrating its efficacy and robustness. Applying hand structure loss (No. 5) further enhances performance over not using it (No. 4), showing its impact on refining hand motion.

We also evaluate a prior mask approach (No. 3), using the union of all pseudo ground truth masks across samples, which underperforms compared to our sample-specific masks (No. 5), highlighting the necessity of our tailored RoM generation in Stage 1.

5. Conclusion

In this paper, we tackle the unique challenges of instructional video generation (IVG) by proposing a novel two-stage method with a tailored hand structure loss. Our approach effectively addresses the challenge of generating accurate subtle hand motion surrounded by cluttered backgrounds through ad-hoc Region of Motion (RoM) mask for each input sample with a diffusion model optimized with the proposed hand structure loss. Extensive experiments demonstrate that our method significantly outperforms four state-of-the-art baselines in generating high-quality instructional videos, both in motion clarity and action relevance. Also, the ablation study demonstrates the effectiveness of each design. This work bridges the gap between video generation techniques and the demands of instructional videos in arbitrary environments for arbitrary action.

References

[1] Niki Aifanti, Christos Papachristou, and Anastasios Delopoulos. The mug facial expression database. In *11th International Workshop on Image Analysis for Multimedia Interactive Services WIAMIS 10*, pages 1–4, 2010. [13](#)

[2] Kumar Ashutosh, Santhosh Kumar Ramakrishnan, Triantafyllos Afouras, and Kristen Grauman. Video-mined task graphs for keystep recognition in instructional videos. *Advances in Neural Information Processing Systems*, 36, 2024. [2](#)

[3] Kumar Ashutosh, Zihui Xue, Tushar Nagarajan, and Kristen Grauman. Detours for navigating instructional videos. In *Proceedings of the IEEE/CVF Conference on Computer Vision and Pattern Recognition*, pages 18804–18815, 2024. [2](#)

[4] Shikhar Bahl, Russell Mendonca, Lili Chen, Unnat Jain, and Deepak Pathak. Affordances from human videos as a versatile representation for robotics. 2023. [2](#)

[5] Max Bain, Arsha Nagrani, Güл Varol, and Andrew Zisserman. Frozen in time: A joint video and image encoder for end-to-end retrieval. In *IEEE International Conference on Computer Vision*, 2021. [13](#)

[6] Yuwei Bao, Keunwoo Yu, Yichi Zhang, Shane Storks, Itamar Bar-Yossef, Alex de la Iglesia, Megan Su, Xiao Zheng, and Joyce Chai. Can foundation models watch, talk and guide you step by step to make a cake? In *Findings of the Association for Computational Linguistics: EMNLP 2023*, pages 12325–12341, 2023. [2](#)

[7] Hugo Bertiche, Niloy J Mitra, Kuldeep Kulkarni, Chun-Hao P Huang, Tuanfeng Y Wang, Meysam Madadi, Sergio Escalera, and Duygu Ceylan. Blowing in the wind: Cyclenet for human cinemagraphs from still images. In *Proceedings of the IEEE/CVF Conference on Computer Vision and Pattern Recognition*, pages 459–468, 2023. [2](#)

[8] Zekun Cao and Regis Kopper. Real-time viewport-aware optical flow estimation in 360-degree videos for visually-induced motion sickness mitigation. In *Proceedings of the 25th Symposium on Virtual and Augmented Reality*, pages 210–218, 2023. [2, 3](#)

[9] Zhi Cen, Huaijin Pi, Sida Peng, Zehong Shen, Minghui Yang, Zhu Shuai, Hujun Bao, and Xiaowei Zhou. Generating human motion in 3d scenes from text descriptions. In *CVPR*, 2024. [4](#)

[10] Paul Chandler and John Sweller. Cognitive load theory and the format of instruction. *Cognition and instruction*, 8(4): 293–332, 1991. [2](#)

[11] Elliot Chane-Sane, Cordelia Schmid, and Ivan Laptev. Learning video-conditioned policies for unseen manipulation tasks. In *ICRA*, 2023. [2](#)

[12] C. Chen, R. Jafari, and N. Kehtarnavaz. UTD-MHAD: A Multimodal Dataset for Human Action Recognition Utilizing a Depth Camera and a Wearable Inertial Sensor. In *Proceedings of IEEE International Conference on Image Processing (ICIP)*, Canada, 2015. [13](#)

[13] Haoxin Chen, Menghan Xia, Yingqing He, Yong Zhang, Xiaodong Cun, Shaoshu Yang, Jinbo Xing, Yaofang Liu, Qifeng Chen, Xiantao Wang, Chao Weng, and Ying Shan. Videocrafter1: Open diffusion models for high-quality video generation, 2023. [3](#)

[14] Haoxin Chen, Yong Zhang, Xiaodong Cun, Menghan Xia, Xiantao Wang, Chao Weng, and Ying Shan. Videocrafter2: Overcoming data limitations for high-quality video diffusion models, 2024. [3](#)

[15] Christian Dornhege, Wolfram Burgard, Christian Zimmermann, Tim Welschendorf, and Thomas Brox. 3d human pose estimation in rgbd images for robotic task learning. In *IEEE International Conference on Robotics and Automation (ICRA)*, 2018. [2](#)

[16] Yung-Yu Chuang, Dan B Goldman, Ke Colin Zheng, Brian Curless, David H Salesin, and Richard Szeliski. Animating pictures with stochastic motion textures. In *ACM SIGGRAPH 2005 Papers*, pages 853–860, 2005. [2](#)

[17] Zuozhuo Dai, Zhenghao Zhang, Yao Yao, Bingxue Qiu, Siyu Zhu, Long Qin, and Weizhi Wang. Fine-grained open domain image animation with motion guidance. *arXiv preprint arXiv:2311.12886*, 2023. [2, 3, 5, 6, 7, 13, 15](#)

[18] Dima Damen, Hazel Doughty, Giovanni Maria Farinella, Antonino Furnari, Evangelos Kazakos, Jian Ma, Davide Moltisanti, Jonathan Munro, Toby Perrett, Will Price, et al. Rescaling egocentric vision: Collection, pipeline and challenges for epic-kitchens-100. *International Journal of Computer Vision*, pages 1–23, 2022. [2, 3, 6, 7, 8, 14, 15](#)

[19] Yilun Du, Sherry Yang, Bo Dai, Hanjun Dai, Ofir Nachum, Josh Tenenbaum, Dale Schuurmans, and Pieter Abbeel. Learning universal policies via text-guided video generation. *Advances in Neural Information Processing Systems*, 36, 2024. [2](#)

[20] Yuki Endo, Yoshihiro Kanamori, and Shigeru Kuriyama. Animating landscape: self-supervised learning of decoupled motion and appearance for single-image video synthesis. *arXiv preprint arXiv:1910.07192*, 2019. [2](#)

[21] Patrick Esser, Johnathan Chiu, Parmida Atighchian, Jonathan Granskog, and Anastasis Germanidis. Structure and content-guided video synthesis with diffusion models. In *Proceedings of the IEEE/CVF International Conference on Computer Vision*, pages 7346–7356, 2023. [4, 5](#)

[22] Tsu-Jui Fu, Licheng Yu, Ning Zhang, Cheng-Yang Fu, Jong-Chyi Su, William Yang Wang, and Sean Bell. Tell me what happened: Unifying text-guided video completion via multimodal masked video generation. In *Proceedings of the IEEE/CVF Conference on Computer Vision and Pattern Recognition*, pages 10681–10692, 2023. [2](#)

[23] Nathan Gavenski, Odinaldo Rodrigues, and Michael Luck. Imitation learning: A survey of learning methods, environments and metrics. *arXiv e-prints*, pages arXiv–2404, 2024. [2](#)

[24] Kristen Grauman, Andrew Westbury, Eugene Byrne, Zachary Chavis, Antonino Furnari, Rohit Girdhar, Jackson Hamburger, Hao Jiang, Miao Liu, Xingyu Liu, et al. Ego4d: Around the world in 3,000 hours of egocentric video. In *Proceedings of the IEEE/CVF Conference on Computer Vision and Pattern Recognition*, pages 18995–19012, 2022. [2, 3, 6, 8, 14, 15](#)

[25] Kristen Grauman, Andrew Westbury, Lorenzo Torresani, Kris Kitani, Jitendra Malik, Triantafyllos Afouras, Kumar

Ashutosh, Vijay Baiyya, Siddhant Bansal, Bikram Boote, et al. Ego-exo4d: Understanding skilled human activity from first-and third-person perspectives. In *Proceedings of the IEEE/CVF Conference on Computer Vision and Pattern Recognition*, pages 19383–19400, 2024. 2

[26] Yuwei Guo, Ceyuan Yang, Anyi Rao, Zhengyang Liang, Yaohui Wang, Yu Qiao, Maneesh Agrawala, Dahua Lin, and Bo Dai. Animatediff: Animate your personalized text-to-image diffusion models without specific tuning. *arXiv preprint arXiv:2307.04725*, 2023. 2, 13

[27] Kaiming He, Xiangyu Zhang, Shaoqing Ren, and Jian Sun. Deep residual learning for image recognition. In *Proceedings of the IEEE conference on computer vision and pattern recognition*, pages 770–778, 2016. 14

[28] Martin Heusel, Hubert Ramsauer, Thomas Unterthiner, Bernhard Nessler, and Sepp Hochreiter. Gans trained by a two time-scale update rule converge to a local nash equilibrium. *Advances in neural information processing systems*, 30, 2017. 6

[29] Jonathan Ho, Ajay Jain, and Pieter Abbeel. Denoising diffusion probabilistic models. *Advances in neural information processing systems*, 33:6840–6851, 2020. 5

[30] Jonathan Ho, Tim Salimans, Alexey Gritsenko, William Chan, Mohammad Norouzi, and David J Fleet. Video diffusion models. In *Advances in Neural Information Processing Systems*, pages 8633–8646. Curran Associates, Inc., 2022. 2

[31] Jonathan Ho, Tim Salimans, Alexey Gritsenko, William Chan, Mohammad Norouzi, and David J Fleet. Video diffusion models. *Advances in Neural Information Processing Systems*, 35:8633–8646, 2022. 2, 5

[32] Aleksander Holynski, Brian L Curless, Steven M Seitz, and Richard Szeliski. Animating pictures with eulerian motion fields. In *Proceedings of the IEEE/CVF Conference on Computer Vision and Pattern Recognition*, pages 5810–5819, 2021. 2

[33] Tim N. Höffler and Detlev Leutner. Instructional animation versus static pictures: A meta-analysis. *Learning and Instruction*, 17(6):722–738, 2007. 5

[34] Vidhi Jain, Maria Attarian, Nikhil J Joshi, Ayzaan Wahid, Danny Driess, Quan Vuong, Pannag R Sanketi, Pierre Sermanet, Stefan Welker, Christine Chan, Igor Gilitschenski, Yonatan Bisk, and Debidatta Dwibedi. Vid2robot: End-to-end video-conditioned policy learning with cross-attention transformers, 2024. 2

[35] Hanwen Jiang, Santhosh Kumar Ramakrishnan, and Kristen Grauman. Single-stage visual query localization in egocentric videos. *Advances in Neural Information Processing Systems*, 36, 2024. 2

[36] Hak Gu Kim, Wissam J Baddar, Heoun-taek Lim, Hyunwook Jeong, and Yong Man Ro. Measurement of exceptional motion in vr video contents for vr sickness assessment using deep convolutional autoencoder. In *Proceedings of the 23rd ACM symposium on virtual reality software and technology*, pages 1–7, 2017. 2, 3

[37] Po-Chen Ko, Jiayuan Mao, Yilun Du, Shao-Hua Sun, and Joshua B Tenenbaum. Learning to act from actionless videos through dense correspondences. In *The Twelfth International Conference on Learning Representations*. 2

[38] Po-Chen Ko, Jiayuan Mao, Yilun Du, Shao-Hua Sun, and Joshua B Tenenbaum. Learning to Act from Actionless Videos through Dense Correspondences. *arXiv:2310.08576*, 2023. 14

[39] Bolin Lai, Xiaoliang Dai, Lawrence Chen, Guan Pang, James M Rehg, and Miao Liu. Lego: Learning egocentric action frame generation via visual instruction tuning. *arXiv preprint arXiv:2312.03849*, 2023. 2, 4, 7, 8, 13

[40] Colin Lea, Michael D Flynn, Rene Vidal, Austin Reiter, and Gregory D Hager. Temporal convolutional networks for action segmentation and detection. In *proceedings of the IEEE Conference on Computer Vision and Pattern Recognition*, pages 156–165, 2017. 5

[41] Yann LeCun, Léon Bottou, Yoshua Bengio, and Patrick Haffner. Gradient-based learning applied to document recognition. *Proceedings of the IEEE*, 86(11):2278–2324, 1998. 5

[42] Junnan Li, Dongxu Li, Caiming Xiong, and Steven Hoi. Blip: Bootstrapping language-image pre-training for unified vision-language understanding and generation. In *International conference on machine learning*, pages 12888–12900. PMLR, 2022. 7, 13

[43] Zhengqi Li, Richard Tucker, Noah Snavely, and Aleksander Holynski. Generative image dynamics. In *Proceedings of the IEEE/CVF Conference on Computer Vision and Pattern Recognition*, pages 24142–24153, 2024. 2

[44] Kevin Qinghong Lin, Jinpeng Wang, Mattia Soldan, Michael Wray, Rui Yan, Eric Z Xu, Difei Gao, Rong-Cheng Tu, Wenzhe Zhao, Weijie Kong, et al. Egocentric video-language pretraining. *Advances in Neural Information Processing Systems*, 35:7575–7586, 2022. 7

[45] Cheng Lu, Yuhao Zhou, Fan Bao, Jianfei Chen, Chongxuan Li, and Jun Zhu. Dpm-solver: A fast ode solver for diffusion probabilistic model sampling in around 10 steps. *Advances in Neural Information Processing Systems*, 35:5775–5787, 2022. 5

[46] Cheng Lu, Yuhao Zhou, Fan Bao, Jianfei Chen, Chongxuan Li, and Jun Zhu. Dpm-solver++: Fast solver for guided sampling of diffusion probabilistic models. *arXiv preprint arXiv:2211.01095*, 2022. 5

[47] Wenquan Lu, Yufei Xu, Jing Zhang, Chaoyue Wang, and Dacheng Tao. Handrefiner: Refining malformed hands in generated images by diffusion-based conditional inpainting. In *ACM Multimedia 2024*, 2024. 2, 5

[48] Camillo Lugaressi, Jiuqiang Tang, Hadon Nash, Chris Mc-Clanahan, Esha Ubweja, Michael Hays, Fan Zhang, Chuo-Ling Chang, Ming Guang Yong, Juhyun Lee, et al. Mediapipe: A framework for building perception pipelines. *arXiv preprint arXiv:1906.08172*, 2019. 3, 5

[49] Priyanka Mandikal and Kristen Grauman. Dexvip: Learning dexterous grasping with human hand pose priors from video. In *Conference on Robot Learning*, 2021. 2

[50] Javier Marin, Aritro Biswas, Ferda Ofli, Nicholas Hynes, Amaia Salvador, Yusuf Aytar, Ingmar Weber, and Antonio Torralba. Recipe1m+: a dataset for learning cross-modal embeddings for cooking recipes and food images. *arXiv preprint arXiv:1810.06553*, 2018. 3

[51] Antoine Miech, Dimitri Zhukov, Jean-Baptiste Alayrac, Makarand Tapaswi, Ivan Laptev, and Josef Sivic. Howto100m: Learning a text-video embedding by watching hundred million narrated video clips. In *Proceedings of the IEEE/CVF international conference on computer vision*, pages 2630–2640, 2019. 3

[52] Suraj Nair, Aravind Rajeswaran, Vikash Kumar, Chelsea Finn, and Abhinav Gupta. R3m: A universal visual representation for robot manipulation. *arXiv preprint arXiv:2203.12601*, 2022. 14

[53] Sudeep Narasimhaswamy, Uttaran Bhattacharya, Xiang Chen, Ishita Dasgupta, Saayan Mitra, and Minh Hoai. Hand-diffuser: Text-to-image generation with realistic hand appearances. In *Proceedings of the IEEE/CVF Conference on Computer Vision and Pattern Recognition*, pages 2468–2479, 2024. 2, 5

[54] Haomiao Ni, Changhao Shi, Kai Li, Sharon X Huang, and Martin Renqiang Min. Conditional image-to-video generation with latent flow diffusion models. In *Proceedings of the IEEE/CVF Conference on Computer Vision and Pattern Recognition*, pages 18444–18455, 2023. 4, 6, 7, 13, 15

[55] Haomiao Ni, Bernhard Egger, Suhas Lohit, Anoop Cherian, Ye Wang, Toshiaki Koike-Akino, Sharon X Huang, and Tim K Marks. Ti2v-zero: Zero-shot image conditioning for text-to-video diffusion models. In *Proceedings of the IEEE/CVF Conference on Computer Vision and Pattern Recognition*, pages 9015–9025, 2024. 2, 3

[56] Alexander Quinn Nichol and Prafulla Dhariwal. Improved denoising diffusion probabilistic models. In *International conference on machine learning*, pages 8162–8171. PMLR, 2021. 2, 5

[57] Konpat Preechakul, Nattanat Chatthee, Suttisak Wizadwongsu, and Supasorn Suwajanakorn. Diffusion autoencoders: Toward a meaningful and decodable representation. In *Proceedings of the IEEE/CVF conference on computer vision and pattern recognition*, pages 10619–10629, 2022. 2

[58] Qin. Dexmv: Imitation learning for dexterous manipulation from human videos, 2021. 2

[59] Alec Radford, Jong Wook Kim, Chris Hallacy, Aditya Ramesh, Gabriel Goh, Sandhini Agarwal, Girish Sastry, Amanda Askell, Pamela Mishkin, Jack Clark, et al. Learning transferable visual models from natural language supervision. In *International conference on machine learning*, pages 8748–8763. PMLR, 2021. 4, 7

[60] Francesco Ragusa, Antonino Furnari, Salvatore Livatino, and Giovanni Maria Farinella. The meccano dataset: Understanding human-object interactions from egocentric videos in an industrial-like domain. In *Proceedings of the IEEE/CVF Winter Conference on Applications of Computer Vision*, pages 1569–1578, 2021. 3

[61] Danilo Jimenez Rezende, Shakir Mohamed, and Daan Wierstra. Stochastic backpropagation and approximate inference in deep generative models. In *International conference on machine learning*, pages 1278–1286. PMLR, 2014. 5

[62] Robin Rombach, Andreas Blattmann, Dominik Lorenz, Patrick Esser, and Björn Ommer. High-resolution image synthesis with latent diffusion models. In *Proceedings of the IEEE/CVF conference on computer vision and pattern recognition*, pages 10684–10695, 2022. 2, 3, 5

[63] Chitwan Saharia, William Chan, Saurabh Saxena, Lala Li, Jay Whang, Emily L Denton, Kamyar Ghasemipour, Raphael Gontijo Lopes, Burcu Karagol Ayan, Tim Salimans, et al. Photorealistic text-to-image diffusion models with deep language understanding. *Advances in neural information processing systems*, 35:36479–36494, 2022. 3

[64] Fadime Sener, Dibyadip Chatterjee, Daniel Shelepor, Kun He, Dipika Singhania, Robert Wang, and Angela Yao. Assembly101: A large-scale multi-view video dataset for understanding procedural activities. In *Proceedings of the IEEE/CVF Conference on Computer Vision and Pattern Recognition*, pages 21096–21106, 2022. 3

[65] Shuai Shen, Wanhu Li, Zheng Zhu, Yueqi Duan, Jie Zhou, and Jiwen Lu. Learning dynamic facial radiance fields for few-shot talking head synthesis. In *European conference on computer vision*, pages 666–682. Springer, 2022. 2

[66] Shuai Shen, Wenliang Zhao, Zibin Meng, Wanhu Li, Zheng Zhu, Jie Zhou, and Jiwen Lu. DiffTalk: Crafting diffusion models for generalized audio-driven portraits animation. In *Proceedings of the IEEE/CVF Conference on Computer Vision and Pattern Recognition*, pages 1982–1991, 2023. 2

[67] Uriel Singer, Adam Polyak, Thomas Hayes, Xi Yin, Jie An, Songyang Zhang, Qiyuan Hu, Harry Yang, Oron Ashual, Oran Gafni, et al. Make-a-video: Text-to-video generation without text-video data. In *The Eleventh International Conference on Learning Representations*. 3

[68] Uriel Singer, Adam Polyak, Thomas Hayes, Xi Yin, Jie An, Songyang Zhang, Qiyuan Hu, Harry Yang, Oron Ashual, Oran Gafni, et al. Make-a-video: Text-to-video generation without text-video data. *arXiv preprint arXiv:2209.14792*, 2022. 5

[69] Yale Song, David Demirdjian, and Randall Davis. Tracking body and hands for gesture recognition: Natops aircraft handling signals database. In *Proceedings of the 9th IEEE International Conference on Automatic Face and Gesture Recognition (FG 2011)*, Santa Barbara, CA, 2011. 13

[70] Achint Soni, Sreyas Venkataraman, Abhranil Chandra, Sebastian Fischmeister, Percy Liang, Bo Dai, and Sherry Yang. Videoagent: Self-improving video generation. *arXiv preprint arXiv:2410.10076*, 2024. 2

[71] Tomáš Souček, Dima Damen, Michael Wray, Ivan Laptev, and Josef Sivic. Genhowto: Learning to generate actions and state transformations from instructional videos. In *2024 IEEE/CVF Conference on Computer Vision and Pattern Recognition (CVPR)*, pages 6561–6571. IEEE, 2024. 2, 4

[72] Shuhan Tan, Tushar Nagarajan, and Kristen Grauman. EgoDistill: Egocentric head motion distillation for efficient video understanding. *Advances in Neural Information Processing Systems*, 36:33485–33498, 2023. 2

[73] Hao Tang, Kevin J Liang, Kristen Grauman, Matt Feiszli, and Weiyao Wang. Egotracks: A long-term egocentric visual object tracking dataset. *Advances in Neural Information Processing Systems*, 36, 2024. 2

[74] Thomas Unterthiner, Sjoerd Van Steenkiste, Karol Kurach, Raphael Marinier, Marcin Michalski, and Sylvain Gelly. To-

wards accurate generative models of video: A new metric & challenges. *arXiv preprint arXiv:1812.01717*, 2018. 7

[75] GÜL VAROL, IVAN LAPTEV, and CORDELIA SCHMID. Long-term temporal convolutions for action recognition. *IEEE transactions on pattern analysis and machine intelligence*, 40(6):1510–1517, 2017. 5

[76] A Vaswani. Attention is all you need. *Advances in Neural Information Processing Systems*, 2017. 5

[77] Xin Wang, Taein Kwon, Mahdi Rad1 Bowen Pan, Ishani Chakraborty, Sean Andrist, Dan Bohus1 Ashley Feniello, Bugra Tekin, Felipe Vieira Frujeri, and Neel Joshi1 Marc Pollefeys. Holoassist: an egocentric human interaction dataset for interactive ai assistants in the real world supplementary material. 3

[78] Xuan Wang, SK Ong, and Andrew Yeh-Ching Nee. Multi-modal augmented-reality assembly guidance based on bare-hand interface. *Advanced Engineering Informatics*, 30(3):406–421, 2016. 2

[79] Xin Wang, Taein Kwon, Mahdi Rad, Bowen Pan, Ishani Chakraborty, Sean Andrist, Dan Bohus, Ashley Feniello, Bugra Tekin, Felipe Vieira Frujeri, et al. Holoassist: an egocentric human interaction dataset for interactive ai assistants in the real world. In *Proceedings of the IEEE/CVF International Conference on Computer Vision*, pages 20270–20281, 2023. 2

[80] Xiang Wang, Hangjie Yuan, Shiwei Zhang, Dayou Chen, Jiniu Wang, Yingya Zhang, Yujun Shen, Deli Zhao, and Jingen Zhou. Videocomposer: Compositional video synthesis with motion controllability. *Advances in Neural Information Processing Systems*, 36, 2024. 2, 4, 5, 13

[81] Jay Zhangjie Wu, Guiyan Fang, Haoning Wu, Xintao Wang, Yixiao Ge, Xiaodong Cun, David Junhao Zhang, Jia-Wei Liu, Yuchao Gu, Rui Zhao, et al. Towards a better metric for text-to-video generation. *arXiv preprint arXiv:2401.07781*, 2024. 7

[82] Wenpeng Xiao, Wentao Liu, Yitong Wang, Bernard Ghanem, and Bing Li. Automatic animation of hair blowing in still portrait photos. In *Proceedings of the IEEE/CVF International Conference on Computer Vision*, pages 22963–22975, 2023. 2

[83] Haofei Xu, Jing Zhang, Jianfei Cai, Hamid Rezatofighi, and Dacheng Tao. Gmflow: Learning optical flow via global matching. In *Proceedings of the IEEE/CVF Conference on Computer Vision and Pattern Recognition*, pages 8121–8130, 2022. 14

[84] Hongwei Xue, Tiankai Hang, Yanhong Zeng, Yuchong Sun, Bei Liu, Huan Yang, Jianlong Fu, and Baining Guo. Advancing high-resolution video-language representation with large-scale video transcriptions. In *International Conference on Computer Vision and Pattern Recognition (CVPR)*, 2022. 13

[85] Zihui Xue, Kumar Ashutosh, and Kristen Grauman. Learning object state changes in videos: An open-world perspective. *arXiv preprint arXiv:2312.11782*, 2023. 2

[86] Chenggang Yan, Yunbin Tu, Xingzheng Wang, Yongbing Zhang, Xinhong Hao, Yongdong Zhang, and Qionghai Dai. Stat: Spatial-temporal attention mechanism for video captioning. *IEEE transactions on multimedia*, 22(1):229–241, 2019. 5

[87] Yashuai Yan, Esteve Valls Mascaro, and Dongheui Lee. Imitationnet: Unsupervised human-to-robot motion retargeting via shared latent space. In *2023 IEEE-RAS 22nd International Conference on Humanoid Robots (Humanoids)*, pages 1–8, 2023. 2

[88] Mengjiao Yang, Yilun Du, Kamyar Ghasemipour, Jonathan Tompson, Dale Schuurmans, and Pieter Abbeel. Learning interactive real-world simulators. *arXiv preprint arXiv:2310.06114*, 2023. 2, 3

[89] Yue Yang, Atith N Gandhi, and Greg Turk. Annotated hands for generative models. *arXiv preprint arXiv:2401.15075*, 2024. 2, 5

[90] Du Yilun, Yang Mengjiao, Dai Bo, Dai Hanjun, Nachum Ofir, Tenenbaum Joshua B, Dale Schuurmans, and Pieter Abbeel. Learning universal policies via text-guided video generation. *arXiv e-prints*, pages arXiv–2302, 2023. 3, 6, 7, 14, 15

[91] Shengming Yin, Chenfei Wu, Jian Liang, Jie Shi, Houqiang Li, Gong Ming, and Nan Duan. Dragnuwa: Fine-grained control in video generation by integrating text, image, and trajectory. *arXiv preprint arXiv:2308.08089*, 2023. 2, 3

[92] Mingyuan Zhang, Zhongang Cai, Liang Pan, Fangzhou Hong, Xinying Guo, Lei Yang, and Ziwei Liu. Motondiffuse: Text-driven human motion generation with diffusion model. *arXiv preprint arXiv:2208.15001*, 2022. 4

[93] Yiming Zhang, Zhenning Xing, Yanhong Zeng, Youqing Fang, and Kai Chen. Pia: Your personalized image animator via plug-and-play modules in text-to-image models. In *Proceedings of the IEEE/CVF Conference on Computer Vision and Pattern Recognition*, pages 7747–7756, 2024. 2, 3, 6, 7, 15

[94] Boyuan Zheng, Sunny Verma, Jianlong Zhou, Ivor W Tsang, and Fang Chen. Imitation learning: Progress, taxonomies and challenges. *IEEE Transactions on Neural Networks and Learning Systems*, 2022. 2

[95] Zangwei Zheng, Xiangyu Peng, Tianji Yang, Chenhui Shen, Shenggui Li, Hongxin Liu, Yukun Zhou, Tianyi Li, and Yang You. Open-sora: Democratizing efficient video production for all, 2024. 13, 14

[96] Luowei Zhou, Chenliang Xu, and Jason Corso. Towards automatic learning of procedures from web instructional videos. In *Proceedings of the AAAI Conference on Artificial Intelligence*, 2018. 2

[97] Luowei Zhou, Chenliang Xu, and Jason J Corso. Towards automatic learning of procedures from web instructional videos. In *AAAI Conference on Artificial Intelligence*, 2018. 3

A. More Qualitative Results Shown in Videos

Most importantly, we invite readers to view more qualitative results in videos in the off-line HTML page attached <https://excitedbutter.github.io/Instructional-Video-Generation/>. An illustration of the page is shown in Fig. 4 for readers’ reference.

By comparing with all baselines, we emphasize three key capabilities of our method that are accountable for the two key designs. Specifically, we observe good performance on generating instructional videos for actions with (i) large hand positional motion (without hallucination in the background); (ii) object state changing; (iii) subtle dexterous fingertip motion. Our proposed learnable automatic Region of Motion mask generation helps the model to focus on the accurate region for the action (“i” and “ii”), avoiding distraction from the cluttered background commonly seen in instructional videos. Our novel hand structure loss helps the model handle the actions with complex but essential fingertip motion (“iii”), which is rarely seen in previous non-instructional video generation benchmarks.

B. Comparison with SOTA Text-to-Video Method

As shown in Tab. 3, we compare with Open-Sora [95], a SOTA Text-to-Video (T2V) generation method since (T2V) has also drawn large attention in the community. However, as we show below T2V is not suitable for Instructional Video generation because it fails to generate the target action in the specific visual context, which is provided the input context image in Text-Image-to-Video (TI2V) work.

C. BLIP Score with Different BLIP Model Size

BLIP Score [39] leverage pre-trained BLIP model [42] to evaluate how close the generated video content is to the target action text description. In the main script, we introduce the evaluation results using the large BLIP model. In this supplementary material, we provide evaluation results from the small BLIP model as well. These results yield the same conclusion as we have in the main script — our method outperforms other baseline methods.

D. Generation of Various Actions in the Same Visual Context

We explore our model’s performance on generating different actions given the same input context image. These are novel image-action pairs that have never shown in the dataset including the test set. We illustrate one example in Fig. 5 that crosses two existing samples in the test set. These results further indicate that our model can generate instructional videos for various actions, emphasizing hand movement and subtle fingertip motion.

E. Baseline Implementation Details

Since previous Text-Image-to-Video/Image Animation work does not report results on the Instructional Video Generation (IVG) task, we implement all four baselines. For a fair comparison, we train or fine-tune their methods on the same training set used for our own method. We provide more details about the implementation as follows:

E.1. Animate Anything

The *Animate Anything* [17] model is initialized from Video-Composer [80], which is pre-trained on the WebVid10M [5] dataset, a large-scale video dataset designed for general video generation tasks. For fine-tuning, the model is trained on 20,000 videos randomly sampled from the HDVILA-100M dataset [84]. These samples are carefully selected to remove watermarks, ensuring higher-quality training data. The model leverages a latent diffusion framework to generate fine-grained animations guided by motion area masks and motion strength.

E.2. Latent Flow Diffusion Model (LFDM)

LFDM [54] is a versatile framework with multiple pre-trained versions. The available pre-training datasets include:

- **The MUG Facial Expression Dataset [1]:** Contains 1,009 videos of 52 subjects performing 7 different facial expressions.
- **The MHAD Human Action Dataset [12]:** Comprises 861 videos of 27 actions performed by 8 subjects.
- **The NATOPS Aircraft Handling Signal Dataset [69]:** Consists of 9,600 videos of 20 subjects performing 24 body-and-hand gestures used for communicating with U.S. Navy pilots.

For the experiments, the version pre-trained on the MHAD Human Action Dataset is used. LFDM generates 8-frame video sequences, employing a two-stage training process: an unsupervised latent flow auto-encoder and a conditional 3D U-Net-based diffusion model for temporal latent flow generation. Training is computationally efficient, requiring only 4 GPUs for a single day of training.

E.3. Personalized Image Animator (PIA)

PIA is trained on the WebVid10M dataset [5], focusing only on the condition module and temporal alignment layers as trainable parameters. The motion module from Animate-Diff [26] is used as a pre-trained model for initializing the temporal alignment layers. PIA fine-tunes on curated images generated by personalized text-to-image (T2I) models, combined with motion-related prompts. These curated images and prompts are included in the AnimateBench benchmark, which consists of diverse images across multiple styles and tailored motion-related annotations. Fine-tuning

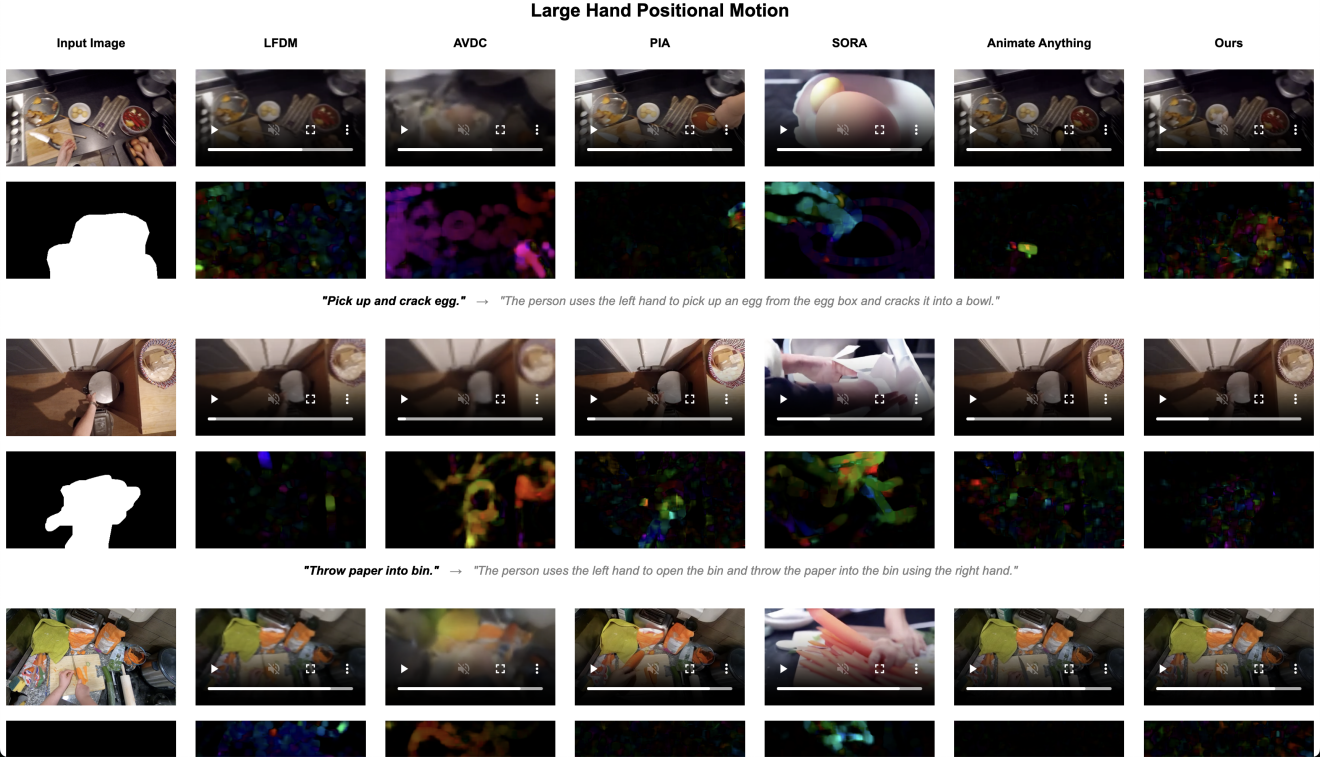


Figure 4. An overview of the HTML page that shows more qualitative results in videos. Please view the full page in attachment <https://excitedbutter.github.io/Instructional-Video-Generation/>

Dataset	Method	HS-Err. \downarrow	GT-Frame		GT-Video		Consistency	Semantic	
			FID \downarrow	CLIP \uparrow	FVD \downarrow	EgoVLP \uparrow		CLIP \uparrow	BLIP.large \uparrow
EpicKitchens	Open Sora [95]	0.01968	135.34	93.823	124.52	0.187	0.9573	24.46	0.186
	Ours	0.01512	5.27	95.904	101.89	0.377	0.9896	31.14	0.298
Ego4D	Open Sora [95]	0.02142	141.90	87.160	117.87	0.252	0.9753	24.12	0.172
	Ours	0.01939	21.51	96.506	103.15	0.664	0.9873	28.63	0.263

Table 3. Comparison our method with a State-of-the-Art Text-to-Video generation method — Open Sora [95]. We show quantitative results on EpicKitchens [18] and Ego4D [24]. Open Sora, representing Text-to-Video methods, is not appropriate for the problem of Instructional Video Generation (IVG) since it fails to generate action demonstration in the specific visual environment. The problem setting of Text-Image-to-Video (TI2V) generation fits more for IVG. Full comparison between our method and SOTA TI2V methods are presented in the main paper.

focuses on the condition module and temporal alignment layers while freezing the base T2I model.

E.4. Actions from Video Dense Correspondences (AVDC)

AVDC [38, 90] is trained on a collection of video datasets featuring table-top manipulation and navigation tasks. Although the specific dataset names are not provided, the training framework synthesizes 8-frame video sequences using a text-conditioned video diffusion model. The weights of the ResNet-18 [27] backbone are initialized either from scratch (BC-Scratch) or using the pre-trained pa-

rameters of R3M [52]. GMFlow [83] is employed for optical flow prediction, enabling dense correspondences for action regression. The model training is computationally optimized to run on 4 GPUs within a single day.

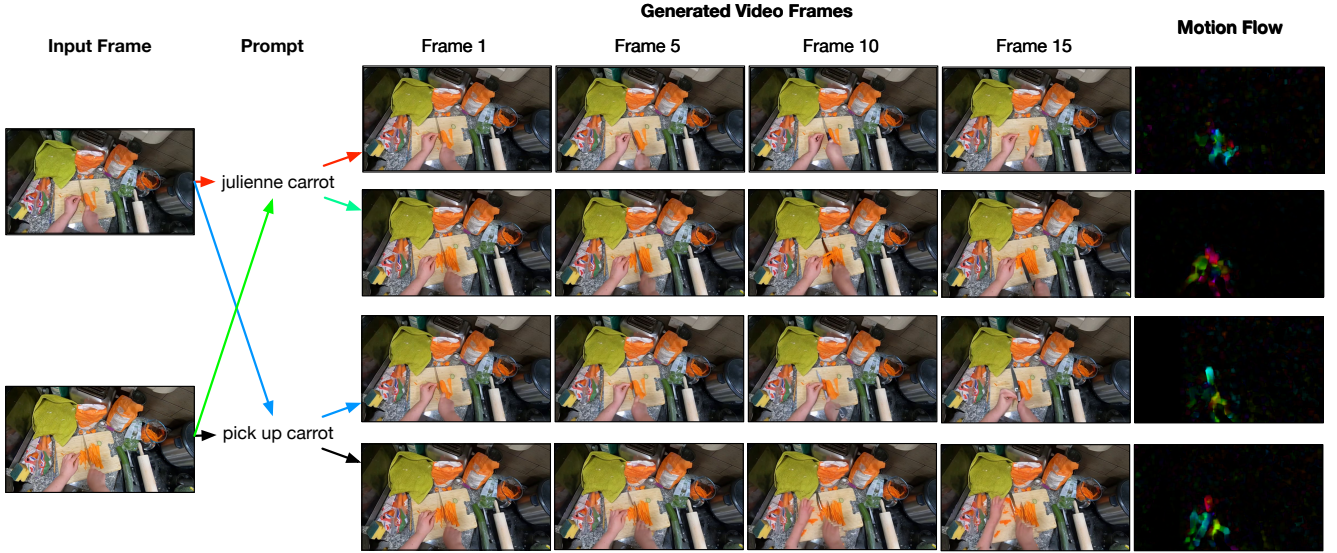


Figure 5. An illustration that crosses the input action text and context image in two test samples. Our method generates reasonable instructional videos for such challenging scenario.

Dataset	Method	BLIP _{large} \uparrow	BLIP _{base} \uparrow
EpicKitchens	LFDM [54]	0.235	0.223
	AA [17]	0.295	0.298
	AVDC [90]	0.116	0.106
	PIA [93]	0.294	0.299
	Ours	0.298	0.335
Ego4D	LFDM [54]	0.221	0.219
	AA [17]	0.260	0.264
	AVDC [90]	0.155	0.161
	PIA [93]	0.219	0.260
	Ours	0.263	0.306

Table 4. Quantitative results on EpicKitchens [18], Ego4D [24] and a Motion Intensive subset of EpicKitchens. Our method outperforms all baselines across all metrics on at least one dataset.